Title: Phenotypic Heterogeneity in Particle Size is a Viral Mechanism of Persistence

Authors: Tian Li[1], Zhenyu Li[1], Meisui Liu[1], Erin E. Deans[1], Tijana Ivanovic[1]*

Affiliations:

[1] Biochemistry Department, Brandeis University, Waltham, MA, USA

*Correspondence to: ivanovic@brandeis.edu

Abstract: Influenza virus particles span ~55-nm to ~30-µm in length, but the role of filamentous particles remains elusive. Filaments package at most a single genome, but display on their surfaces disproportionately more hemagglutinins (HAs). During cell entry, 3-5 neighboring HAs form a fusion cluster, delivering the genome across the endosomal membrane. Here we identify influenza filaments as viral persisters increasing the probability of fusion-cluster formation and cell entry under HA-directed selective pressure. When HA function is limited, filamentous particles fuse more rapidly and more efficiently than do spherical ones, but their infectious advantage derives from their enhanced fusion efficiency rather than from rate effects. Filaments are refractory to extreme HA inactivation, presenting a built-in reservoir of particles that can adapt to any condition limiting HA function.

One Sentence Summary: Filamentous virus particles resist inhibition at the level of membrane fusion in the absence of genetic change.

Main Text:

Many enveloped animal viruses and some emerging human pathogens such as Ebola, Nipah, and Hendra viruses, produce a mixture of virus-particle sizes that include very long, filamentous members(*1-4*). However, the function of the filamentous particles is unknown for any system. The main impediments to characterizing viral filaments are their phenotypic origin (a single infecting particle gives rise to a range of particle sizes)(*5, 6*), difficulty of purifying particles to homogeneity according to their size, and the apparent lack of filament advantage *in vitro(7, 8)*. Influenza filaments are advantageous and persist *in vivo*, but are quickly replaced by spherical particles during virus passaging *in vitro(9, 10)*. Spherical particles are taken up by cells via clathrin-mediated endocytosis, and filaments via a slower and more energy-requiring macropinocytosis(*11*). Furthermore, the assembly of filaments takes up tremendous resources (e.g. membranes and viral proteins), but they package the same, single-genome cargo(*12-14*). It is thus

assumed that to understand the benefit of viral filaments, a full complexity of *in-vivo* infections needs to be considered.

The relative simplicity of virus structure offers hints into the filament function. Influenza virus has three structural proteins whose numbers scale with particle size: the matrix protein, M1, which forms the particle shape, and the surface-exposed HA and NA(*12, 14*). HA densely covers at least 80% of the viral surface and its relative representation is higher on longer particles at the expense of NA(*6, 12, 14*). HA is the main target of neutralizing antibodies and is thus under constant pressure to evolve(*15*). Furthermore, adaptation of HA to human-cell entry is a key determinant of influenza pandemics, so viral zoonotic transmission is another source of selective pressure on HA(*16*). Presentation of HA on particles of different sizes might offer an adaptability benefit, and detailed dissection of HA function in different particle contexts should reveal its mechanism.

Increased infectivity of filamentous particles under HA pressure

We used filamentous influenza virus, X31HA/Udorn(*17*), and devised a strategy for particle size-enrichment using cycles of centrifugation at low relative centrifugal force, which preferentially sediments filamentous particles. We analyzed the resultant fractions by negative-stain electron microscopy (Fig. S1A-B, and Table S1). The supernatant fraction (SUP) has a relatively narrow and symmetric particle-size distribution, with 95% of the population ranging in length from 50 nm to 250 nm. Taking 250 nm as the cut off, the pellet fraction (PELLET) includes 47.2% filaments, whose average length is ~5-times that of the SUP particles (Table S1).

To produce a variable, measurable limit to HA activity, we used a Fab fragment of a broadly neutralizing antibody, MEDI8852 (M-Fab), which binds the base of HA and prevents HA conformational changes(*18*). Fluorescently tagged M-Fab binding to unlabeled particles shows a

narrow distribution of particle intensities for the SUP particles, and a wider fluorescence-intensity distribution with a long tail for the PELLET particles (Fig. S2A). M-Fab binding thus scales with particle length. Incubation of M-Fab-bound particles at low pH did not significantly change fluorescence-intensity distributions (Fig. S2A), validating M-Fab as a reagent that inactivates targeted HA during membrane fusion at the low-pH of endosomes.

To determine whether viral filaments offer infectivity advantage under HA-directed selective pressures, we measured the SUP- and PELLET-particle concentrations (in hemagglutination units per ml; HAU/ml) needed to induce 50% cell death for a range of M-Fab concentrations in a single-cycle of infection ($scTCID_{50}$) (Fig. 1). We limited infections to a single cycle because particle-size separation is possible only for the initial infection, which then yields pleomorphic progeny(*5, 6*). In the absence of inhibition, the PELLET has no infectivity advantage (and in some experiments a subtle disadvantage) over the SUP (Fig. 1A), consistent with previous reports for viral filaments(*7, 8*). However, the effect of M-Fab on the $scTCID_{50}$ of the PELLET is lower than its effect on the SUP, with the PELLET advantage ranging from 50% (17 nM M-Fab) to greater than 3-fold (268 nM M-Fab) (Fig. 1B). The $scTCID_{50}$ data show that influenza virus sensitivity to HA inhibition decreases with increase in virus-particle length.

Prediction from stochastic simulations for the function of filamentous particles

HA is synthesized as an inactive trimer, HA0(*19*). Activation requires cleavage of each HA0 monomer into two disulfide-linked subunits, HA1 and HA2(*20*). The contact interface (patch) between the virus particle and the membrane incorporates ~50 HAs for the spherical particles, and this number scales approximately linearly with particle length(*12, 14, 17*) (Fig. 2A). Membrane fusion results from a functional interplay among HAs within the contact patch. Cleaved HA is metastable; low pH reduces the barrier for transition to the stable postfusion

conformation(*21*). Initial HA triggering is stochastic, but inducing membrane merger requires the combined free energy released by the HA conformational changes of 3-5 neighboring trimers(*17, 22*) (Fig. 2A). A hydrophobic sequence at the N-terminus of HA2, termed the fusion peptide (FP), mediates functional coupling of HA conformational changes to membrane fusion. In the pre-fusion HA, FP inserts in a conserved cavity (the pre-fusion pocket) at the base of HA near the viral membrane(*19*). During HA conformational changes in the contact patch, FP either inserts into the target membrane (productive HA), or, if HA assumes the post-fusion state without engaging the target membrane, FP inserts back into the viral membrane (unproductive HA)(*22, 23*). The release of FP from the pre-fusion pocket is the rate-limiting structural rearrangement influencing the rate of fusion-cluster formation(*17*). The frequency of unproductive HAs, which imposes restrictions on the available geometries for adjacent HA insertions, influences the rate and probability of fusion-cluster formation(*22, 24*). While membrane resistance prevents individual inserted HAs from folding back, the fold-back for HAs in the fusion cluster is cooperative and fast(*17*).

The larger contact patch afforded by viral filaments should increase the total number of inserted HAs and thus the efficiency and/or rate of membrane fusion under any condition limiting HA activity, e.g. large fraction of unproductive HA, low level of HA0 activation, or HA inactivation by antibodies or inhibitors (Fig. 2A). To express these predictions in quantitative terms, we performed stochastic simulations of fusion for a 600-fold range of patch sizes and zero to 80-97% HA inactivation (Fig. 2B). The probability of fusion-cluster formation for spherical particles (PS 55) declines for HA inactivation greater than 20%, but a 600-times larger patch (PS 34627) requires at least 90% HA inactivation for the same effect, and yields 20% fusion for 97% inactive HAs. Larger patches form fusion clusters more rapidly, but rate differences get smaller

for more HA inactivation. Overall, larger patch enables higher efficiency and/or rate of fusion-cluster formation depending on the extent of HA inactivation.

Functional advantage of filamentous particles revealed by single-particle measurements of membrane fusion

To compare the predictions from stochastic simulations with experiment, we used the SUP and PELLET fractions of WT X31HA/Udorn in single-particle experiments of membrane fusion. Analysis of individual particles can reveal subpopulations with distinct kinetics, and in this way, obviate the need for homogeneous particle preparations. We performed membrane fusion experiments with DiD-labeled SUP or PELLET particles on supported planar membrane bilayers for a range of unlabeled M-Fab concentrations at pH5.2 (Movie S1-S4). We extracted individual-particle lag times from pH drop to hemifusion (onset of DiD dequenching), a fusion intermediate that reports on fusion-cluster formation and invariably precedes pore opening(*17, 25*) (Fig. 3A). We fitted frequency distributions of hemifusion lag times with gamma probability density and derived mean lag times from the fits(*22, 25*). The plots of hemifusion yield and time for a range of M-Fab concentrations both show that the PELLET particles are less sensitive to HA inactivation than the SUP particles (Fig. 3B). We derived hemifusion yield and lag-time distributions for the long (>250 nm) particles within the PELLET (Fig. 3C) as described in the Materials and Methods. The resultant plots of SUP versus long particles match the prediction from stochastic simulations for patch-size pairs where the larger patch size is ~4-5 times the size of the smaller one (e.g. 55/235 or 121/583) (Fig. 2B); the derived patch-size ratio in turn agrees with the measured ratio of the filament and SUP-particle average lengths (Table S1). The combined results thus validate the stochastic fusion model(*22*), and support the prediction that the larger patch afforded by viral filaments increases the rate and probability of fusion-cluster formation under limiting HA activity.

Effect of HA inactivation on infectivity

The infectious advantage of filaments for a given level of HA inactivation (Fig. 1) could stem from their increase in the fusion rate, yield, or both. To test whether kinetics of fusion-cluster formation influences infectivity outcomes, we employed virus mutants with (de)stabilized pre-fusion HA. A mutation in HA2, $D112_2A$, destabilizes FP in its pre-fusion pocket resulting in faster hemifusion(*17*). A mutation in HA1, $H17_1Y$, stabilizes FP in its pre-fusion pocket and is predicted to slow hemifusion(*26*). The extent of fluorescent M-Fab binding to WT and $D112_2A$ particles is the same, and to $H17_1Y$ only slightly reduced, implying the same or very similar extent of HA inactivation for a given M-Fab concentration (Fig. S2B). Indeed, single-particle measurements for WT and $D112_2A$ give very similar hemifusion-yield curves, and a similar relative change in hemifusion lag-times (Fig. 4A, S3A). However, $D112_2A$ particles are 7 to 11 times faster in hemifusion for the tested range of M-Fab concentrations, owing to the faster rate of fusion-peptide release for the mutant(*17*). At even the highest M-Fab concentration, hemifusion of $D112_2A$ particles is 2.4-fold faster than that of the uninhibited WT (Fig. 4A, S3A). $H17_1Y$, on the other hand, is so stabilized that it has lower hemifusion yield at pH 5.2, either because of a lower extent of HA triggering or lower productiveness (Fig. 4A). At pH 4.8, hemifusion yield of $H17_1Y$ is comparable to WT, but hemifusion rate is markedly lower for the mutant (Fig. 4B, S3B). Unlike the large changes in the rate of hemifusion for HA mutations, even the highest concentration of M-Fab tested slows hemifusion of the short particles less than 5-fold (Fig. 3B, 4A-B). Thus, the HA mutants allow us to probe the effects of altered hemifusion-rates on infectivity.

We compared WT, $D112_2A$, and $H17_1Y$ viruses in $scTCID_{50}$ experiments (Fig. 4C-E, S4). The baseline titers of $D112_2A$ and $H17_1Y$ viruses are within 2-3-fold of WT, showing that cell entry is relatively insensitive to the rate of fusion-cluster formation (Fig. 4C). Furthermore, WT

and D112$_2$A viruses are equally sensitive to all tested M-Fab concentrations, confirming that the rate increase afforded by HA destabilization does not boost infectivity under HA pressure (Fig. 4D). H17$_1$Y is more sensitive to HA inactivation than WT and D112$_2$A viruses, but otherwise follows the same trend for the higher M-Fab concentration (Fig. 4D). The higher sensitivity of H17$_1$Y to M-Fab can be interpreted in the context of this mutant's lower hemifusion yield at the pH of endosomes (Fig. 4A). If the lower rate of fusion-cluster formation for H17$_1$Y contributed to its higher sensitivity to M-Fab, a further increase in M-Fab concentration would inhibit H17$_1$Y disproportionately, causing it deviate from the WT/D112$_2$A infectivity curves. The same infectivity trend for H17$_1$Y confirms that cell entry of even the slow-fusing H17$_1$Y mutant is insensitive to rate changes caused by HA inactivation (Fig. 4D). M-Fab thus lowers infectivity by reducing the number of particles that successfully assemble fusion clusters.

Filaments resist extreme HA inactivation

The unproductive HA fraction contributes to the overall probability of virus particles assembling fusion clusters and determines how sensitive particles will be to HA inactivation (Fig. 2A)(*22, 24*). The effect of M-Fab on fusion-cluster formation in endosomes (Fig. 4D) is much greater than its effect *in vitro* (Fig. 4A). For example, 67 nM of M-Fab reduces scTCID$_{50}$ titers 14-fold for the WT and D112$_2$A SUP particles, but hemifusion-yield changes are comparably small for this M-Fab concentration *in vitro*. Productive HAs are thus less frequent in endosomes than on planar membrane bilayers, and inactivation of a small subset of HAs prevents a majority of virus particles in endosomes from assembling fusion clusters.

The effect of M-Fab on the scTCID$_{50}$ of D112$_2$A or H17$_1$Y PELLET (Fig. 4E) is lower than its effect on the corresponding SUP (Fig. 4D), with PELLET advantage being the same for the mutants as for the WT. We interpret PELLET advantage as resulting from more opportunities

for fusion-cluster formation on longer particles (Fig. 2A). This interpretation predicts that infectivity differences between PELLET and SUP fractions would be greater for such HA-inactivation extents that start to affect very long filaments because PELLET and SUP particle distributions are more different for longer particles (Table S2). To test this prediction, we prepared virus particles with less than 1% activating HA0 cleavage (Fig. 5A). We then measured the loss of infectivity for the uncleaved virus, or the uncleaved virus pre-treated with 268 nM M-Fab, relative to fully cleaved, untreated virus in a modified plaque-assay experiment (Fig. 5B). The result for the control (cleaved, M-Fab pre-treated) virus matched the scTCID$_{50}$ data at this M-Fab concentration (Fig. 1) with the PELLET offering approximately 3-fold higher infectivity than the SUP (Fig. 5B). A similar result was obtained for the uncleaved virus. Consistent with our prediction for extreme HA pressure, the uncleaved, M-Fab pre-treated PELLET is at least 10-times more infectious than the corresponding SUP. Since at really high HA inactivation levels the rate of fusion-cluster formation approaches a plateau (Fig. 2,3), this result supports our interpretation that the PELLET advantage derives from an increase in the fusion yield. Our results thus define influenza filaments as viral persisters under general HA pressures (presence of inhibitors and/or near absence of activating HA cleavage).

Discussion

Our results show that the bulk of endosomal fusion is unproductive and exquisitely sensitive to small perturbations in active-HA numbers. Filaments resist HA inactivation by having more opportunities for fusion-cluster formation. Very long filaments enable cell entry when active HAs become extremely rare independent of the reasons for low HA-function; they replicate without requiring genetic change, and in this way, accumulate mutations that can lead to (genetic) adaptation.

We propose a model for viral particle-size diversity serving as a phenotypic switch in changing environment (Fig. 6). At low relative HA-directed selective pressure, majority of new infections are initiated by spherical particles; they are more numerous, use fewer resources, and are faster to internalize and assemble (Fig. 6A)(*6, 8*). Filaments take over when HA function is limiting and permit low level of replication (Fig. 6B). If pressure is removed, the same viral population can expand. Under sustained pressure, viral replication initiated by filaments can lead to adaptive mutations. For example, filaments might enable low level of replication under immune pressure, and even permit inefficiencies in HA function for immune evasion mutants, which can then be repaired by mutation. Similarly, cell entry by the early zoonotic transgressors in humans might be permitted by the filamentous virus population, in turn allowing for adaptive mutations.

Targeting filamentous influenza particles should extend the effectiveness of vaccinations or fusion inhibitors, as well as help curb viral pandemics arising from adaptation of new influenza strains. One way to achieve that is to target the molecular pathways that enable filament assembly. For example, NA inhibitors disproportionately affect the release of filaments because of the higher relative NA-content on spherical particles(*6*). Combining HA and NA inhibitors might thus delay resistance in an unanticipated way because NA pressure increases the proportion of spherical particles, ready targets for HA inhibitors. An attractive target for delaying resistance to HA pressures might also lie in the unique cell biology of large-cargo internalization (i.e. macropinocytosis) (Fig. 6C)(*11, 27-31*). Targeting cellular factors required for filamentous-virus internalization would both curb avenues for resistance by targeting host processes, and provide broad-spectrum effect against filamentous virus pathogens(*1-4*).

References and Notes:

1. A. J. Battisti *et al.*, Structure and assembly of a paramyxovirus matrix protein. *Proc Natl Acad Sci U S A* **109**, 13996-14000 (2012).

2. T. A. Bharat *et al.*, Structural dissection of Ebola virus and its assembly determinants using cryo-electron tomography. *Proc Natl Acad Sci U S A* **109**, 4275-4280 (2012).
3. A. D. Hyatt, S. R. Zaki, C. S. Goldsmith, T. G. Wise, S. G. Hengstberger, Ultrastructure of Hendra virus and Nipah virus within cultured cells and host animals. *Microbes Infect* **3**, 297-306 (2001).
4. L. Liljeroos, M. A. Krzyzaniak, A. Helenius, S. J. Butcher, Architecture of respiratory syncytial virus revealed by electron cryotomography. *Proc Natl Acad Sci U S A* **110**, 11133-11138 (2013).
5. C. M. Chu, I. M. Dawson, W. J. Elford, Filamentous forms associated with newly isolated influenza virus. *Lancet* **1**, 602 (1949).
6. M. D. Vahey, D. A. Fletcher, Low-Fidelity Assembly of Influenza A Virus Promotes Escape from Host Cells. *Cell* **176**, 678 (2019).
7. P. C. Roberts, R. A. Lamb, R. W. Compans, The M1 and M2 proteins of influenza A virus are important determinants in filamentous particle formation. *Virology* **240**, 127-137 (1998).
8. B. Dadonaite, S. Vijayakrishnan, E. Fodor, D. Bhella, E. C. Hutchinson, Filamentous influenza viruses. *J Gen Virol* **97**, 1755-1764 (2016).
9. P. W. Choppin, J. S. Murphy, I. Tamm, Studies of two kinds of virus particles which comprise influenza A2 virus strains. III. Morphological characteristics: independence to morphological and functional traits. *J Exp Med* **112**, 945-952 (1960).
10. J. Seladi-Schulman, J. Steel, A. C. Lowen, Spherical influenza viruses have a fitness advantage in embryonated eggs, while filament-producing strains are selected in vivo. *J Virol* **87**, 13343-13353 (2013).
11. J. S. Rossman, G. P. Leser, R. A. Lamb, Filamentous influenza virus enters cells via macropinocytosis. *J Virol* **86**, 10950-10960 (2012).
12. L. J. Calder, S. Wasilewski, J. A. Berriman, P. B. Rosenthal, Structural organization of a filamentous influenza A virus. *Proc Natl Acad Sci U S A* **107**, 10685-10690 (2010).
13. T. Noda *et al.*, Architecture of ribonucleoprotein complexes in influenza A virus particles. *Nature* **439**, 490-492 (2006).
14. S. Wasilewski, L. J. Calder, T. Grant, P. B. Rosenthal, Distribution of surface glycoproteins on influenza A virus determined by electron cryotomography. *Vaccine* **30**, 7368-7373 (2012).
15. C. A. Russell *et al.*, The global circulation of seasonal influenza A (H3N2) viruses. *Science* **320**, 340-346 (2008).
16. C. M. Mair, K. Ludwig, A. Herrmann, C. Sieben, Receptor binding and pH stability - how influenza A virus hemagglutinin affects host-specific virus infection. *Biochim Biophys Acta* **1838**, 1153-1168 (2014).
17. T. Ivanovic, J. L. Choi, S. P. Whelan, A. M. van Oijen, S. C. Harrison, Influenza-virus membrane fusion by cooperative fold-back of stochastically induced hemagglutinin intermediates. *Elife* **2**, e00333 (2013).
18. N. L. Kallewaard *et al.*, Structure and Function Analysis of an Antibody Recognizing All Influenza A Subtypes. *Cell* **166**, 596-608 (2016).
19. J. Chen *et al.*, Structure of the hemagglutinin precursor cleavage site, a determinant of influenza pathogenicity and the origin of the labile conformation. *Cell* **95**, 409-417 (1998).

20. I. A. Wilson, J. J. Skehel, D. C. Wiley, Structure of the haemagglutinin membrane glycoprotein of influenza virus at 3 A resolution. *Nature* **289**, 366-373 (1981).
21. P. A. Bullough, F. M. Hughson, J. J. Skehel, D. C. Wiley, Structure of influenza haemagglutinin at the pH of membrane fusion. *Nature* **371**, 37-43 (1994).
22. T. Ivanovic, S. C. Harrison, Distinct functional determinants of influenza hemagglutinin-mediated membrane fusion. *Elife* **4**, e11009 (2015).
23. S. A. Wharton *et al.*, Electron microscopy of antibody complexes of influenza virus haemagglutinin in the fusion pH conformation. *EMBO J* **14**, 240-246 (1995).
24. J. J. Otterstrom *et al.*, Relating influenza virus membrane fusion kinetics to stoichiometry of neutralizing antibodies at the single-particle level. *Proc Natl Acad Sci U S A* **111**, E5143-5148 (2014).
25. D. L. Floyd, J. R. Ragains, J. J. Skehel, S. C. Harrison, A. M. van Oijen, Single-particle kinetics of influenza virus membrane fusion. *Proc Natl Acad Sci U S A* **105**, 15382-15387 (2008).
26. S. Thoennes *et al.*, Analysis of residues near the fusion peptide in the influenza hemagglutinin structure for roles in triggering membrane fusion. *Virology* **370**, 403-414 (2008).
27. E. de Vries *et al.*, Dissection of the influenza A virus endocytic routes reveals macropinocytosis as an alternative entry pathway. *PLoS Pathog* **7**, e1001329 (2011).
28. A. Nanbo *et al.*, Ebolavirus is internalized into host cells via macropinocytosis in a viral glycoprotein-dependent manner. *PLoS Pathog* **6**, e1001121 (2010).
29. M. F. Saeed, A. A. Kolokoltsov, T. Albrecht, R. A. Davey, Cellular entry of ebola virus involves uptake by a macropinocytosis-like mechanism and subsequent trafficking through early and late endosomes. *PLoS Pathog* **6**, e1001110 (2010).
30. M. A. Krzyzaniak, M. T. Zumstein, J. A. Gerez, P. Picotti, A. Helenius, Host cell entry of respiratory syncytial virus involves macropinocytosis followed by proteolytic activation of the F protein. *PLoS Pathog* **9**, e1003309 (2013).
31. O. Pernet, C. Pohl, M. Ainouze, H. Kweder, R. Buckland, Nipah virus entry can occur by macropinocytosis. *Virology* **395**, 298-311 (2009).
32. T. Ivanovic *et al.*, Kinetics of proton transport into influenza virions by the viral M2 channel. *PLoS One* **7**, e31566 (2012).
33. X. Zhang *et al.*, Features of reovirus outer capsid protein mu1 revealed by electron cryomicroscopy and image reconstruction of the virion at 7.0 Angstrom resolution. *Structure* **13**, 1545-1557 (2005).
34. I. Chen, B. M. Dorr, D. R. Liu, A general strategy for the evolution of bond-forming enzymes using yeast display. *Proc Natl Acad Sci U S A* **108**, 11399-11404 (2011).
35. J. Diao *et al.*, A single vesicle-vesicle fusion assay for in vitro studies of SNAREs and accessory proteins. *Nat Protoc* **7**, 921-934 (2012).
36. J. Larson *et al.*, Design and construction of a multiwavelength, micromirror total internal reflectance fluorescence microscope. *Nat Protoc* **9**, 2317-2328 (2014).
37. R. S. Daniels *et al.*, Fusion mutants of the influenza virus hemagglutinin glycoprotein. *Cell* **40**, 431-439 (1985).

Acknowledgments: We thank Goran Bajic (Harvard Medical School) for help with Fab expression and purification, Milos Popovic (Boston University) for help with analysis codes, and Stephen C. Harrison (Harvard Medical School), Bruce L. Goode (Brandeis University), and Amy

Lee (Brandeis University) for comments on the manuscript; **Funding:** We acknowledge support from the NIH Director's New Innovator Award to TI, 1DP2GM128204, and the NSF MRSEC DMR-1420382; **Author contributions:** TL, Experiment design, Acquisition of data, Analysis and interpretation of data; ZL, ML, ED, Acquisition of data, Analysis and interpretation of data; TI, Conception and design, Experiment design, Acquisition of data, Analysis and interpretation of data, Writing of the manuscript. **Competing interests:** Authors declare no competing interests; **Data and materials availability:** All data are available in the main text or the supplementary materials. Raw numbers used for plotting or additional movie files are available from the authors upon request. The MATLAB codes used for stochastic simulations are available at eLIFE with the DOI: 10.7554/eLife.11009. The MATLAB codes for fusion data analysis are available at eLIFE with the DOI: 10.7554/eLife.00333 and the DOI:10.7554/eLife.11009. The MATLAB codes used for fluorescence-intensity analysis are included in the supplementary information files.

Supplementary Materials:

Materials and Methods

Figures S1-S4

Tables S1-S2

Movies S1-S4

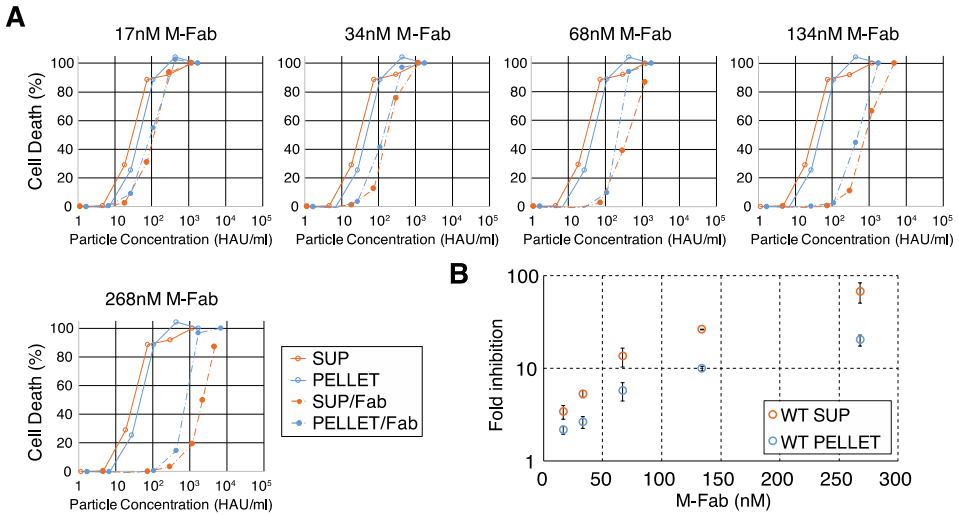

Fig. 1. Filamentous particles have an infectivity advantage under HA inhibition. (A) A representative set of scTCID$_{50}$ measurements at various M-Fab concentrations. The no-inhibitor baseline for PELLET and SUP from which infectivity shifts are measured in (B) is shown on all plots. (B) Fold decrease in scTCID$_{50}$ titer for M-Fab-treated samples relative to untreated samples. Average and standard deviation of three independent experiments are shown.

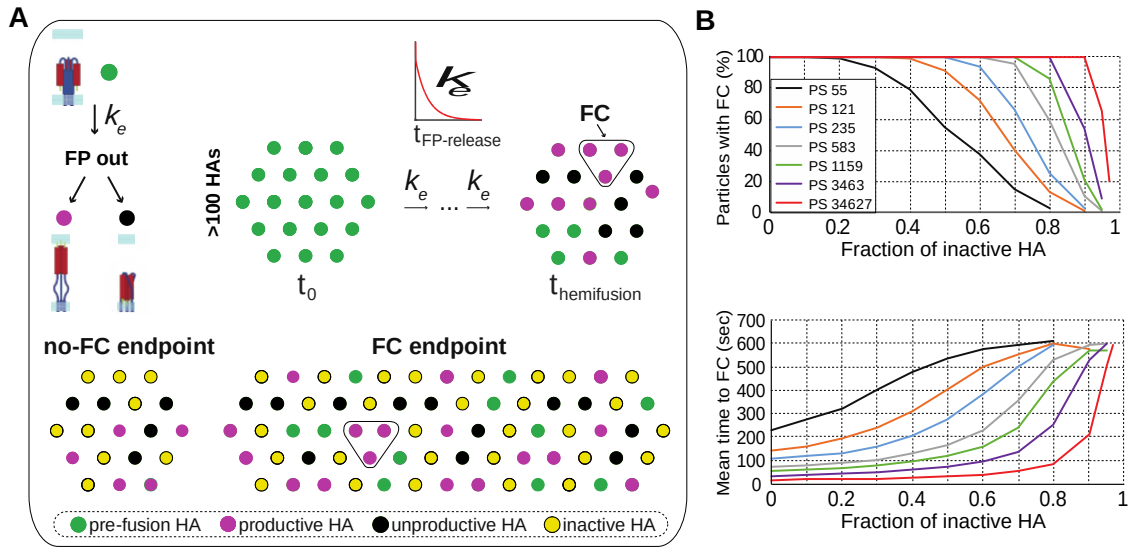

Fig. 2. Stochastic simulations. (A) Stochastic fusion model(*22*). A simplified contact patch before fusion (t_0) or at the time of fusion-cluster (FC) formation ($t_{hemifusion}$) is shown (*top*). Random HAs extend and insert into the target membrane (pre-fusion HA, green circles; inserted HA, magenta circles) or become inactivated (unproductive HA, black circles). k_e is the rate of FP release. Under the same limiting condition, longer particles have a higher probability of fusion-cluster formation (*bottom*). Inactive (inhibitor bound or uncleaved) HAs are shown as yellow circles. The prediction for the advantage of filamentous particles is illustrated with an elliptical patch, but the simulations used circular patches (see Materials and Methods). (B) Simulation results for the yield and mean lag-time to fusion-cluster formation at 0.02-0.1 inactive HA-fraction increments connected with lines from datasets each with at least 1000 FCs. PS, patch size represented with the number of HA molecules interfacing the target membrane.

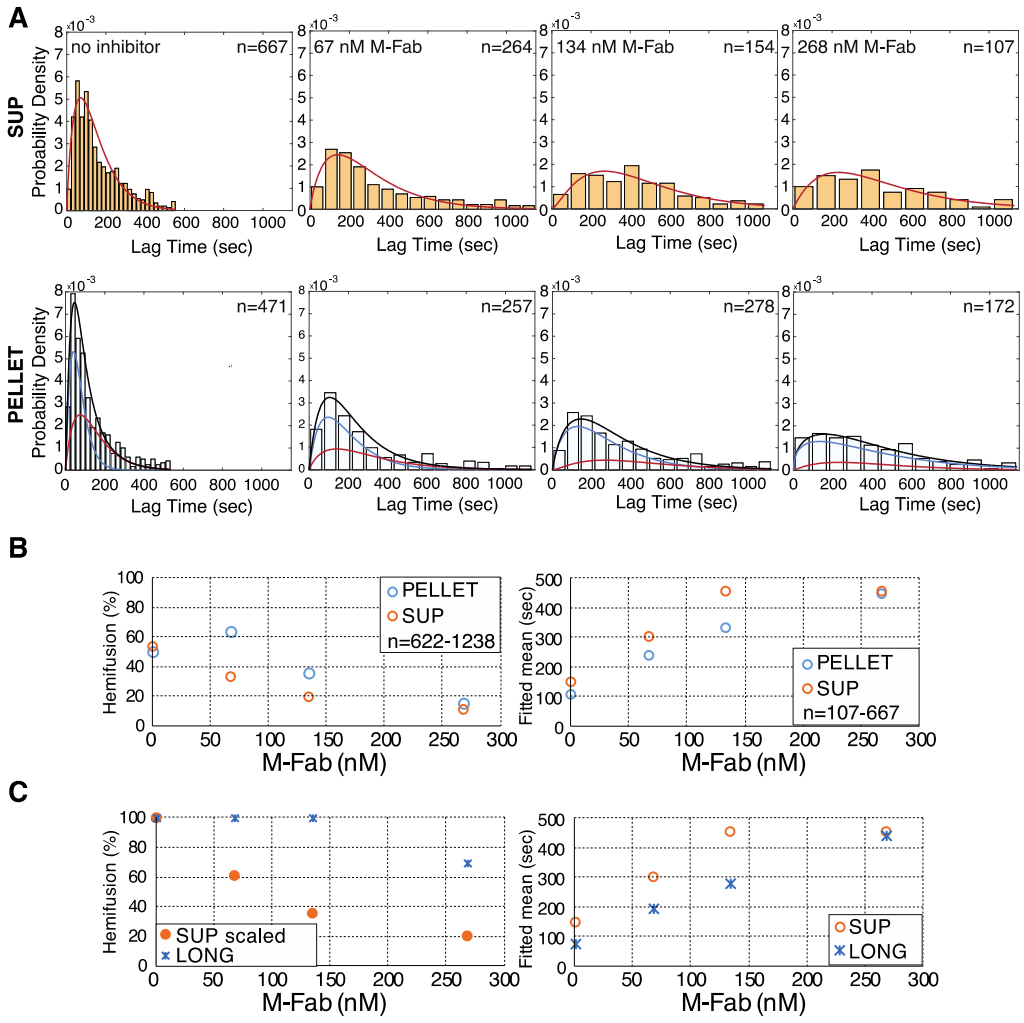

Fig. 3. Single-particle membrane fusion of short and long particles. (A) Hemifusion lag times with gamma-distribution fit (SUP, *red line*), or bi-gamma fit (PELLET, *black line*) with the underlying distributions for the short (*red line*) and long (*blue line*) PELLET-particle subpopulations. Data were pooled from several experiments where each condition was represented on each day. (B) Hemifusion yield, and fitted mean from (A). (C) Derived hemifusion yield and fitted mean for long particles in the PELLET (see Materials and Methods).

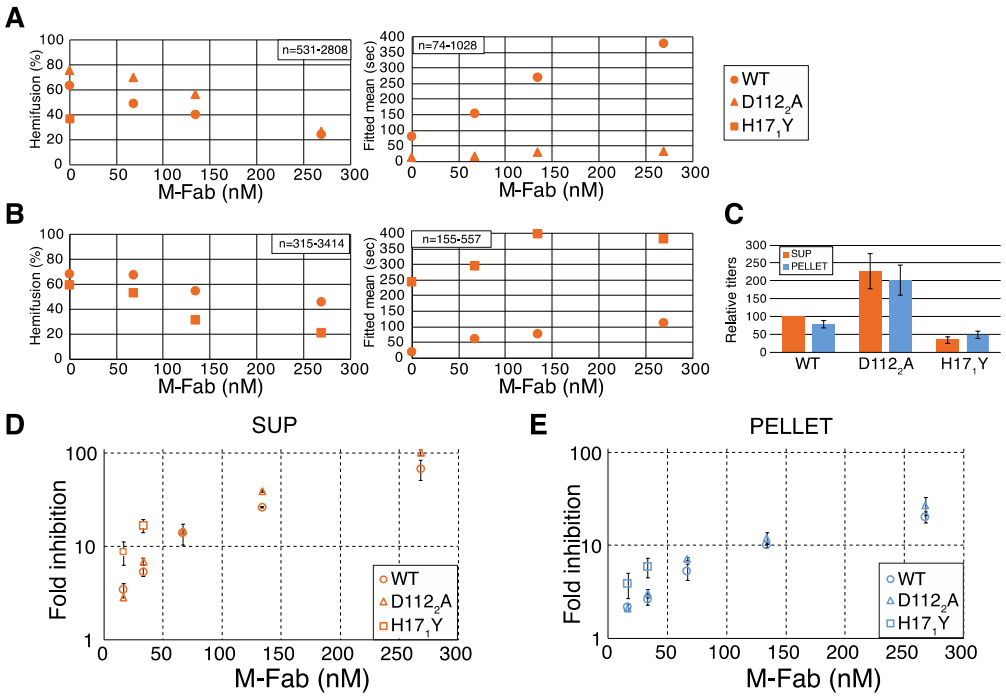

Fig. 4. HA inhibition reduces the number of particles assembling fusion clusters during endosomal fusion. (A-B) Single-particle hemifusion yield and fitted mean for a range of M-Fab concentrations for short particles, (A) WT versus D112$_2$A and a single H17$_1$Y data point at pH 5.2, and (B) WT versus H17$_1$Y at pH 4.8. (C) Baseline scTCID$_{50}$ titers normalized to WT SUP. Average and standard deviation of three independent experiments are shown. (D-E) Fold decrease in scTCID$_{50}$ titer for M-Fab-treated samples relative to untreated samples for (D) SUP or (E) PELLET of WT, D112$_2$A, and H17$_1$Y viruses. Average and standard deviation of three independent experiments are shown. WT data is replotted from Fig. 1B for direct comparison.

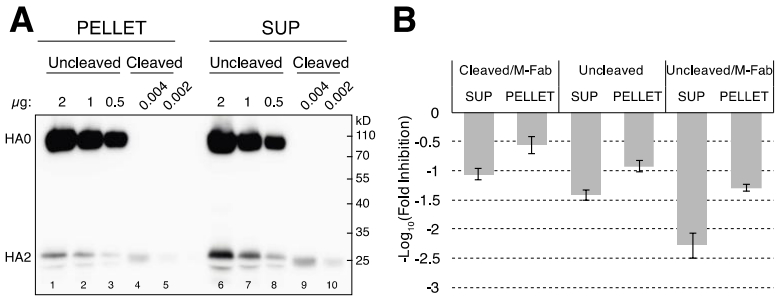

Fig. 5. Filaments resist extreme HA inactivation. (A) HA2 Western blot of purified virus particles. µg refers to the total viral protein loaded. (B) Fold reduction in recovered infectivity (plaque-forming units) per input particle (HAU) for uncleaved and/or 268 nM M-Fab treated samples, relative to cleaved, untreated samples. The experiment was set up in a way to ensure that any differences among samples result from the initial infection by the SUP and PELLET fractions (see Materials and Methods). Data is the average and standard deviation of three independent measurements.

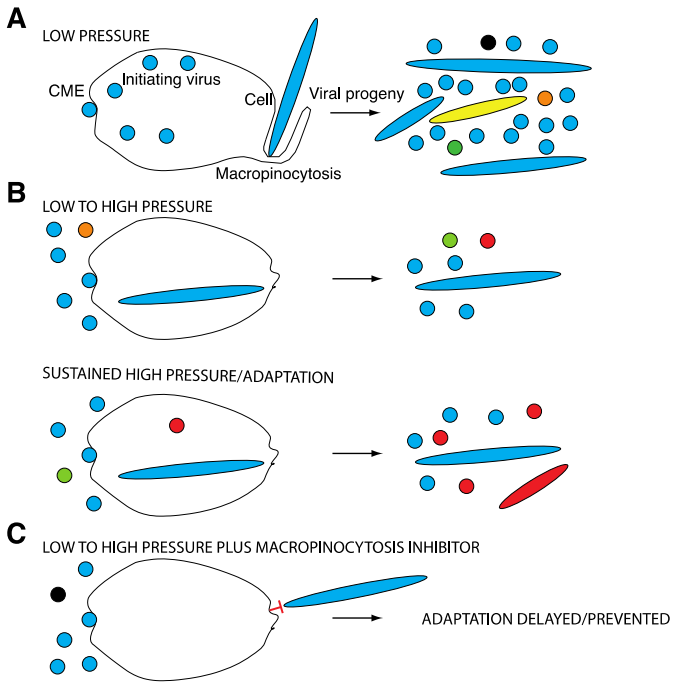

Fig. 6. A model for the influenza virus phenotypic switch. Viral progeny is pleomorphic independent of the initiating-virus morphology. Random mutations arise during replication. (A) At low HA pressure, infections by spherical particles dominate. (B) Filamentous particles permit cell entry and replication when spherical particles are inhibited, and can lead to adaptive mutations. (C) Preventing macropinocytosis in combination with HA inactivation by inhibitors might avert resistance. The same strategy might apply to prolonging vaccine effectiveness or preventing zoonotic adaptations that can lead to pandemics. Circles, spherical particles; Ellipses, filaments; Blue, WT; Black/Orange/Green, HA mutants; Red, an adaptive HA mutant; CME, clathrin-mediated endocytosis.